Direct numerical simulation of flame stabilization assisted by autoignition in a reheat gas turbine combustor

Konduri Aditya[a,*], Andrea Gruber[b], Chao Xu[c], Tianfeng Lu[c], Alex Krisman[a], Mirko R. Bothien[d], Jacqueline H. Chen[a]

[a]*Combustion Research Facility, Sandia National Laboratories, Livermore, CA, USA*
[b]*SINTEF Energy Research, Trondheim, Norway*
[c]*Department of Mechanical Engineering, University of Connecticut, Storrs, USA*
[d]*Ansaldo Energia Switzerland, Baden, Switzerland*

Abstract

A three-dimensional direct numerical simulation (DNS) is performed for a turbulent hydrogen-air flame, represented with detailed chemistry, stabilized in a model gas-turbine combustor. The combustor geometry consists of a mixing duct followed by a sudden expansion and a combustion chamber, which represents a geometrically simplified version of Ansaldo Energia's GT26/GT36 sequential combustor design. In this configuration, a very lean blend of hydrogen and vitiated air is prepared in the mixing duct and convected into the combustion chamber, where the residence time from the inlet of the mixing duct to the combustion chamber is designed to coincide with the ignition delay time of the mixture. The results show that when the flame is stabilized at its design position, combustion occurs due to both autoignition and flame propagation (deflagration) modes at different locations within the combustion chamber. A chemical explosive mode analysis (CEMA) reveals that most of the fuel is consumed due to autoignition in the bulk-flow along the centerline of the combustor, and lower amounts of fuel are consumed by flame propagation near the corners of the sudden expansion, where the unburnt temperature is reduced by the thermal wall boundary layers. An unstable operating condition is also identified, wherein periodic auto-ignition events occur within the mixing duct. These events appear upstream of the intended stabilization position, due to positive temperature fluctuations induced by pressure waves originating from within the combustion chamber. The present DNS investigation represents the initial step of a comprehensive research effort aimed at gaining detailed physical insight into the rate-limiting processes that govern the sequential combustor behavior and avoid the insurgence of the off-design auto-ignition events.

Keywords: sequential combustor, flame stabilization, autoignition, hydrogen, direct numerical simulation

1. Introduction

There is an increasing interest in the use of hydrogen (H_2) for power generation. H_2 can reduce carbon emissions from fossil fuels in carbon capture and storage (CCS) systems and can provide an energy storage solution for power-to-gas-to-power schemes that will complement the increasing share of non-dispatchable renewable energy resources.

The reheat concept, first implemented in Alstom's GT24/GT26 gas turbines [1] and then further developed into Ansaldo Energia's Constant Pressure Sequential Combustor [2], is presently integrated into the H-class GT36 engine (see Fig. 1). It consists of two combustor stages that operate at lean premixed conditions. The first stage is aerodynamically stabilized by vortex breakdown and flame propagation. The second stage is stabilized primarily by autoignition in the *sequential* or *reheat* combustor, but premixed flame propagation (deflagration) may also assist flame stabilization near the recirculation zones which are at a reduced temperature due to heat loss to the relatively cold walls.

The reheat design is able to provide fuel-flexibility, which is achieved by varying the loading of each combustor stage separately: for highly reactive fuels such as H_2, the first-stage combustor can operate stably at a lower flame temperature compared to standard natural gas operation. This in turn reduces the inlet temperature to the second stage sequential combustor, which

*Corresponding author: Konduri Aditya
Email address: akonduri@sandia.gov (Konduri Aditya)

This is the accepted version of an article published in Proceedings of the Combustion Institute.
DOI: 10.1016/j.proci.2018.06.084

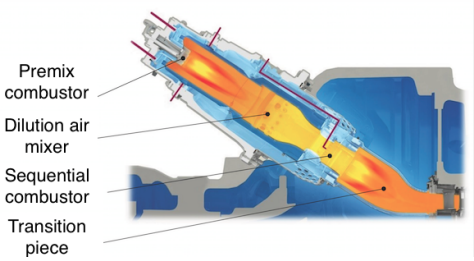

Figure 1: Schematic of the GT36's two-stage combustion system (courtesy of Ansaldo Energia).

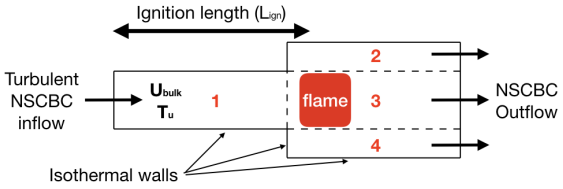

Figure 2: The computational domain, boundary conditions and the multi-block arrangement.

counteracts the fuel reactivity effect on the auto-ignition delay time [1]. By shifting the fuel from the first to the second stage, high H_2 fuel content can be burned without de-rating the engine, i.e. without efficiency and power losses which pose a significant advantage when compared to single stage combustor, as discussed in [3]. Turbulent combustion in the sequential combustor occurs under very unique conditions, i.e. with vitiated oxidant, elevated pressures (up to $\sim 20\,bar$) and high reactant temperatures ($> 1000\,K$). Because of the specificity of these conditions, few relevant studies are available in the literature. An interesting series of papers have reported pressurized laboratory experiments conducted at the Institute of Combustion Research of DLR on a scaled, simplified version of the sequential combustor [4–6]. However, these experimental studies offer a limited picture of the reheat combustion process in the main flame since they focused on the formation of auto-ignition kernels in the mixing duct. While a few numerical studies have considered hydrogen and methane combustion at reheat conditions [3, 7, 8], these investigations considered only simplified zero-dimensional (0D) or one-dimensional (1D) reactor models and focused mainly on ignition and propagation time scales as a theoretical complement to the planning and execution of full-scale, high-pressure experiments. A very recent large-eddy simulation (LES) study [9] has attempted the quantification of the auto-ignition process that characterizes a simple, widely-validated laboratory flame configuration (Berkeley flame [10]) using a methodology originally suggested in [11]. Other recent numerical studies investigated the dynamic response of the auto-ignition flame using LES to extract the flame transfer function (FTF) [12–14] but did not attempt to provide detailed insight of the reheat combustion process itself. Recently, a LES study of flame dynamics in a reheat sequential combustor with methane fuel injection was reported in [15].

The present work represents the first attempt to gain fundamental insight into the hydrogen-air combustion process in a model sequential combustor utilizing massively-parallel three-dimensional (3D) direct numerical simulation (DNS), detailed chemical kinetics and chemical explosive modes analysis (CEMA) at reheat conditions. The most notable exception to nominal reheat conditions in this first DNS study is that pressure is assumed to be at atmospheric conditions for computational expediency. More specifically, the objective of this study is to identify and elucidate the structure and stabilization mechanism of the turbulent flame which is subjected to auto-ignitive conditions, wall heat transfer, and flow recirculation.

2. Simulation details

Figure 2 shows the multi-block model configuration used for the sequential combustor in the present study, with each block numbered 1–4. Block 1 represents the mixing duct and blocks 2–4 represent the combustion chamber. The mixing duct is followed by a sudden expansion (duct cross-sectional area change) into the sequential combustion chamber. The multi-block implementation preserves the numerical accuracy of the underlying numerical methods, and is based on the code S3D which is a high-order accurate combustion DNS solver [16]. S3D solves the governing Navier-Stokes, conservation of mass, energy and species mass fractions with 8^{th}-order central finite difference approximations for spatial derivatives and a 4^{th}-order six-stage explicit Runge-Kutta scheme for integrating the solution in time. The solution is filtered at each time step with a 10^{th}-order explicit filter [17, 18].

The relative dimensions of the upstream mixing duct are $3L\times L\times 1.5L$ in the x (streamwise), y (cross stream), and z (spanwise) directions, respectively, where L is the wall-to-wall width of the mixing duct. The relative dimensions of the combustion chamber are $3L\times 2L\times 1.5L$. The physical dimensions of the DNS domain are chosen such that auto-ignition of the reactants mixture entering the domain from the upstream inlet takes place at the

This is the accepted version of an article published in Proceedings of the Combustion Institute.
DOI: 10.1016/j.proci.2018.06.084

flame design position within the combustion chamber and downstream of the sudden expansion (area change): $L_{ign} = 4 \times L \sim U_{bulk} \times t_{ign}$, where U_{bulk} is the bulk flow velocity in the mixing duct, t_{ign} and L_{ign} are the ignition delay time and the "ignition length", respectively, for the reactants' mixture composition and temperature. Similar to the experimental investigations [6], the bulk velocity U_{bulk} is set to $200m/s$ while the normalization length scale L is set to $1cm$, resulting in an overall domain size that represents the upper limit for what is computationally feasible today.

A structured, uniform Cartesian grid is used for all blocks with a spatial resolution $\Delta s = \Delta x = \Delta y = \Delta z = 20\mu m$ and a total mesh count of 1.25 billion. The chosen spatial resolution resolves the thinnest radical layers throughout the domain with at least ten points across the thinnest front and provides a marginal resolution of the viscous length scale at the wall $\Delta s \sim \delta_v$. The inflow and outflow boundary conditions are imposed as a non-reflecting inlet (on the left-hand side of block 1) and a non-reflecting outlet (right-hand side of blocks 2–4) according to the Navier-Stokes characteristic boundary condition (NSCBC) method described in [19]. A periodic (cyclic) boundary condition is imposed in the z (spanwise) direction for all blocks to enforce a homogeneous direction that facilitates sampling of statistics. All other boundaries are set to no-slip, iso-thermal walls using the methodology described in [20] and maintained at a constant temperature $T_w = 750K$ in order to account for the effect of effusion wall cooling on the reactants' flow, and thereby on the flame stabilization mechanism.

The homogeneous mixture of fuel and vitiated oxidant (taken as the products of the first H_2-air combustion stage at $\phi = 0.43$ and $T = 773K$) enters the domain from the upstream inlet of the mixing duct as a fully developed turbulent channel flow at Reynolds number $Re_\tau = 378$ based on the viscous length scale δ_v ($Re_b \sim 13,000$ based on the channel bulk velocity) and it is characterized by an equivalence ratio of $\phi = 0.35$ and preheat temperature $T_u = 1100K$. The selected reactants' temperature and composition are similar to those utilized in the experimental investigations conducted at DLR [6]. A separate, auxiliary DNS of a corresponding non-reacting fully developed turbulent channel flow is used to generate the most realistic fluctuating velocity field for the inlet of the reacting case. This well established methodology [21–23] ultimately provides the nominal bulk velocity U_{bulk} in the mixing duct that, together with the imposed inflow temperature T_u, results in the desired induction time t_{ign} and length L_{ign} as described above.

The 3D DNS simulation is initialized with field data from a non-reacting 2D simulation extruded in the spanwise direction to minimize the simulation time required to flush out initial transient artifacts from the domain. Once the non-reacting flow reaches a fully developed state, a burnt products composition is imposed in the combustion chamber based on a progress variable parametrization of the laminar flame that nominally describes combustion at the conditions investigated ($\phi = 0.35$ and $T_u = 1100K$). It is assumed that the new (reactive flow) transient artifacts are flushed out of the computational domain after one full transit time t_T. This quantity is estimated to be approximately $t_T \sim 0.28ms$ in the present geometry before the sampling of the solution is started.

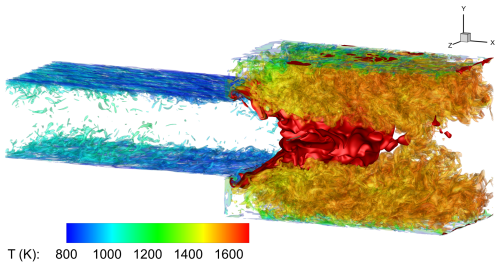

Figure 3: Illustration of instantaneous flow field represented by iso-surfaces of vorticity magnitude at 300000 1/s colored by the enclosed temperature scale. The flame shape and location within the combustion chamber is illustrated by the red iso-surface of a representative value of heat release rate.

The hydrogen-air chemistry is represented with a detailed 9 species, 21 reaction chemical mechanism by Li *et al.* [24]. Transport properties are evaluated on a mixture-averaged basis and the Soret effect (thermal diffusion) is included given its importance for hydrogen flames at low equivalence ratios in particular. An instantaneous 3D flow field from the simulation is shown in Fig. 3.

3. Combustion mode indicator based on Chemical Explosive Mode Analysis (CEMA)

A new quantitative diagnostic based on the chemical explosive mode analysis (CEMA) is applied and used alongside *ad hoc* methods based on a transport budget analysis [25] for selected species normal to reaction fronts, to differentiate between the distinct autoignition and flame propagation combustion modes present in the sequential mixing and combustor sections. The CEMA [26, 27] is a flame diagnostic based on eigen-analysis of the Jacobian of the local chemical source term in the

This is the accepted version of an article published in Proceedings of the Combustion Institute.
DOI: 10.1016/j.proci.2018.06.084

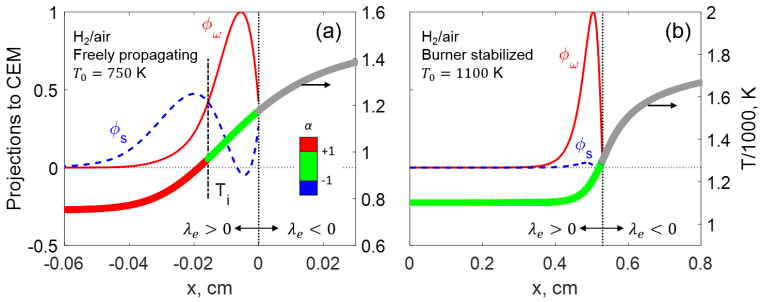

Figure 4: Profiles of chemical and diffusion projection terms together with the temperature profiles for (a) a freely-propagating premixed flame at T_u=750 K, and (b) a burner-stabilized flame at T_u=1100 K, for a hydrogen/air mixture at atmospheric pressure.

governing equation of a reacting flow:

$$\frac{D\omega(\mathbf{y})}{Dt} = \mathbf{J}_\omega \frac{D\mathbf{y}}{Dt} = \mathbf{J}_\omega(\omega + \mathbf{s}) \, , \mathbf{J}_\omega = \frac{\partial \omega}{\partial \mathbf{y}} \tag{1}$$

where $\mathbf{y}$ is the vector of local dependent variables including temperature and species concentrations, ω is the chemical source term and $\mathbf{s}$ is a non-chemical source term such as diffusion in reacting flows. It has been shown in previous work [26, 27] that the chemical explosive mode (CEM) associated with a positive eigenvalue of the chemical Jacobian indicates that the local mixture tends to ignite if the mixture is isolated [26]. CEM is present in pre-ignition mixtures and disappears past ignition, as such the zero-crossing of the eigenvalue is associated with critical flame features, such as ignition, extinction, and a premixed reaction front, which change the mixtures explosive property. CEMA is extended to distinguish between different combustion modes [28], where Eq. 1 is projected to the direction of the left eigenvector of CEM, $\mathbf{b}$:

$$\mathbf{b} \cdot \frac{D\omega(\mathbf{y})}{Dt} = \mathbf{b} \cdot \mathbf{J}_\omega(\omega + \mathbf{s}) = \lambda_\mathbf{e} \mathbf{b} \cdot (\omega + \mathbf{s}) \tag{2}$$

$$\frac{D\phi_\omega}{Dt} = \lambda_\mathbf{e}\phi_\omega + \lambda_\mathbf{e}\phi_\mathbf{s} + \frac{D\mathbf{b}}{Dt} \cdot \omega(\mathbf{y}) \tag{3}$$

where the projected chemical and non-chemical source terms are denoted as $\phi_\omega = \mathbf{b} \cdot \omega(\mathbf{y})$ and $\phi_s = \mathbf{b} \cdot \mathbf{s}(\mathbf{y})$, respectively. Therefore, the ratio $\alpha = \phi_s/\phi_\omega$ indicates how important the diffusion source term is to the CEM compared with the chemical source term. A positive α indicates that the non-chemical source term is promoting ignition. Based on the values of α, the following modes are identified: assisted-ignition ($\alpha > 1$), which occurs where diffusion significantly promotes reaction; auto-ignition ($-1 < \alpha < 1$), which occurs when chemistry plays a dominant role; and local extinction ($\alpha < -1$), which occurs when diffusion dominates chemistry and suppresses ignition.

Figure 3 shows the profiles of the projected chemical and diffusion source terms for a freely-propagating premixed flame at T_u=750 K (Fig. 3a), and a burner-stabilized flame at T_u=1100 K (Fig. 3b), for a hydrogen/air mixture at atmospheric pressure. It is seen that for a deflagration wave at T_u=750 K, diffusion dominates chemistry, i.e., $\alpha > 1$, for the region where T<T_i with T_i representing the crossover point of ϕ_ω and ϕ_s. In contrast, for the burner-stabilized flame at T_u=1100 K, chemical reaction dominates diffusion, i.e., $-1 < \alpha < 1$, for all explosive mixtures ($\lambda_e > 0$), indicating that the flame is an auto-ignition front. In the present study, the CEMA-based criterion is employed to distinguish different local combustion modes in the DNS.

4. Results

A first important observation from the DNS dataset reveals the existence of two temporally alternating combustion *states* in the model sequential combustor under investigation. In the primary and most (statistically) prominent state, a triangular-shaped flame is stabilized in the combustion chamber immediately downstream of the area change as qualitatively illustrated by the instantaneous plots in Fig. 5. In a secondary periodically intermittent combustion state, auto-ignition of the reactants occurs in the mixing duct well upstream of the area change. While the former combustion state, described in greater detail in Sec. 4.1, represents the design target operation mode of the sequential combustor, the latter intermittent combustion state is caused by early auto-ignition of the highly-reactive hydrogen fuel resulting in an off-design location of the combustion process (see Sec. 4.2 for details). In order to ensure engine operation with sufficient margin, tests at engine conditions are conducted in practice to find the inlet temperature threshold that results in a stable flame

This is the accepted version of an article published in Proceedings of the Combustion Institute.
DOI: 10.1016/j.proci.2018.06.084

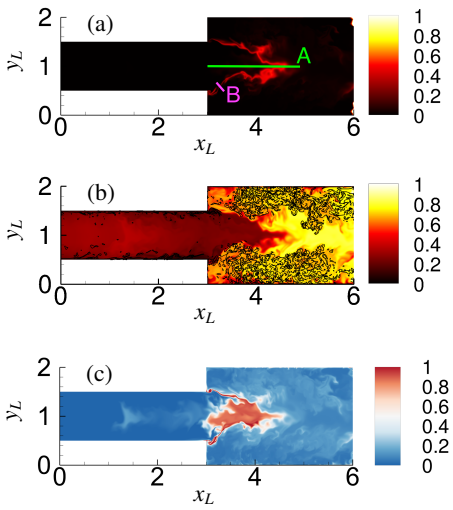

Figure 5: Flame stabilization in combustion chamber - iso-contours of normalized heat release rate (a), temperature (b), and HO_2 mass fraction (c) for the same instantaneous snapshot of the solution are shown on 2-D slices of the computational domain (at the mid-plane in the spanwise direction). The black iso-lines in part (b) represent the value of vorticity magnitude, 250000 1/s. The transport budget terms in Figure 6 are evaluated along the lines A and B shown in part (a) of this figure.

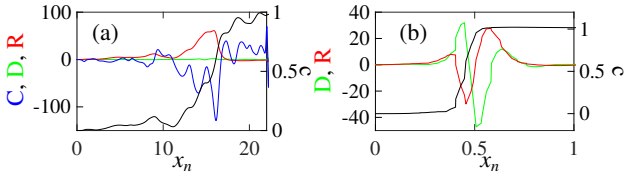

Figure 6: Instantaneous transport budget terms of OH species normal to (a) auto-ignition front and (b) flame propagation. Lines represent: c - progress variable (black), C - convection (blue), D - diffusion (green), and R - reaction (red). x_n is the normal distance.

confined to the combustion chamber. Qualitative observations and quantitative physical insights obtained from the present detailed simulations are used to complement the experimental results and achieve better understanding of the complex reacting flow that characterizes the sequential combustor.

4.1. Design combustion state

The two principal combustion modes present at the design combustion state are a deflagration wave (premixed flame) and an auto-ignition controlled process characterized by variable speed dependent upon the local residence time, resulting in a triangular-shaped combustion zone illustrated in Fig. 5. The deflagration mode arises due to a complex interaction between the heat transfer to the walls and aerodynamic recirculation. Due to the heat loss to the cold walls, the temperature of the reactants in the near-wall region of the mixing duct is lower than in the bulk flow. This inhibits the ability of reactants in the near-wall region to auto-ignite in the combustion chamber. However, the flow separation caused by the sudden expansion creates the necessary recirculation region of hot products and radicals in the corners, resulting in a flame propagation that consumes the reactants advected from the near-wall region into the combustion chamber.

The instantaneous contours of normalized quantities of heat release rate, temperature and mass fraction of HO_2 are illustrated in Fig. 5. The heat release rate and HO_2 mass fraction are normalized by their peak values in the domain, and the temperature by the adiabatic flame temperature value evaluated at 1 atm and 1100 K. Figure 5 (a) shows that the heat release rate in the flame propagation mode is relatively low and occurs in thin regions immediately downstream of the area change, while the bulk part of the heat release arises in a volumetrically-distributed auto-ignition mode. This is also consistent with the greater temperature rise near the centerline post combustion region, observed in Fig. 5 (b). Note that the presence of shear layers, evident from the iso-lines of vorticity magnitude in the figure, promote the cooling effect from the cold isothermal walls by enhancing lateral mixing. In addition to the contribution from heat release, the temperature rise in the post combustion region is also affected by this cooling effect, which is stronger near the walls and decreases towards the centerline. Hence, the greater temperature rise across the flame along the centerline is also due to the reduced cooling effect from the walls at the centerline. In the ignition of hydrogen-air at the simulation conditions, HO_2 is a key radical that is produced in the nearly isothermal chemical chain branching step preceding thermal runaway. Clearly, the iso-contours of the HO_2 mass fraction in Fig. 5 (c) indicate its formation upstream of the heat release rate along the centerline and in the thin regions just downstream of the area change. There HO_2 is produced and consumed within a thin preheat layer of a premixed flame.

Figure 6 presents a transport budget analysis of OH performed along two lines, A and B, normal to the local reaction fronts at a particular instance in time, as indicated in Fig. 5 (a). Figure 6 (a), shows that the budget evaluated along line A consists of a balance between convection and the reaction with negligible contribution from diffusion, as is expected in the case of auto-ignition. Figure 6 (b) shows the instantaneous transport

This is the accepted version of an article published in Proceedings of the Combustion Institute.
DOI: 10.1016/j.proci.2018.06.084

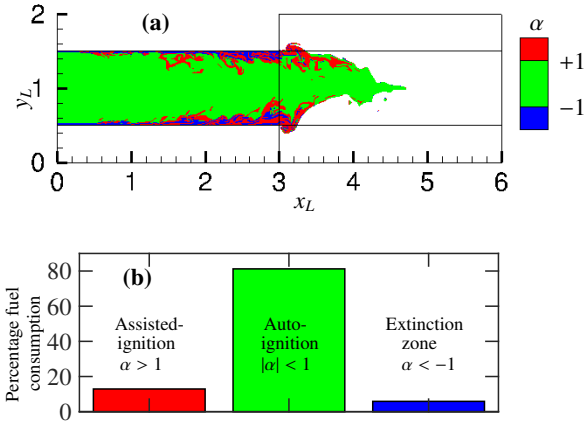

Figure 7: (a) Iso-contours of the instantaneous field of α delineating the combustion modes: autoignition $|\alpha| < 1$ (green), assisted-ignition $\alpha > 1$ (red), extinction zone $\alpha < -1$ (blue). (b) Bar chart quantifying the fraction of H_2 fuel consumption (reaction rate) due to each mode.

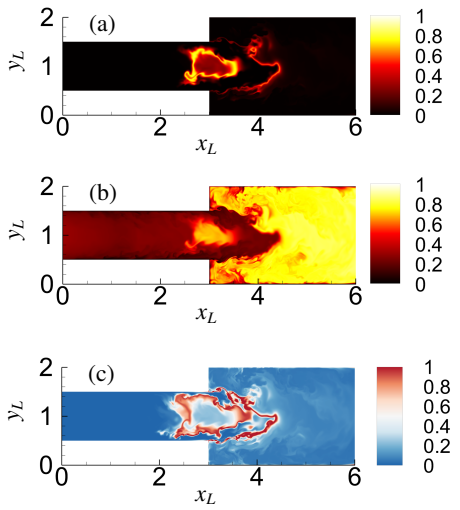

Figure 8: Auto-ignition event in the mixing duct: iso-contours of normalized heat release rate (a), temperature (b) and HO_2 mass fraction (c) for the same instantaneous snapshot of the solution are shown in 2-D slices of the computational domain (at the midplane in the spanwise direction).

budget along line B near the lower corner of the sudden expansion, which reveals a diffusion–reaction balance, characteristic of a deflagration wave. The convection term, in this case, has a significant value across the flame and balances the unsteady term. Hence, this term is not shown in the graph for the sake of clarity.

The new criterion based on the chemical explosive mode analysis (CEMA), outlined in Sec. 3, is applied to further distinguish between the two different combustion modes present in the mixing duct and the combustion chamber. The CEMA diagnostics project the local diffusion and reaction source terms in the direction of the chemical explosive mode (CEM) such that the relative importance of reaction and diffusion, aligned with the CEM, can be quantified. Figure 7 (a) shows iso-contours of the instantaneous values of the CEM local combustion mode indicator α in a spanwise midplane slice through the three-dimensional data. The value of α determines the relative importance of chemical reactions and diffusion. In the bulk flow of the mixing duct, and in the triangular shaped combustion zone in the combustion chamber, the magnitude of α is less than unity signifying the presence of an autoignition mode (green-colored regions). On the other hand, near the boundary layers of the mixing duct and in the combustion chamber, immediately downstream of the area change, the magnitude of α is greater than unity in the flame's preheat layers (red-colored regions) signifying that flame propagation (where it actually happens) is assisted locally by ignition. Finally, the blue-colored regions within the boundary layers and just downstream of the area change represents magnitudes of α less than -1, the so-called "extinction mode" where diffusion overwhelms reaction, thereby suppressing the propensity to ignite. The H_2 fuel consumption (reaction rate) in each of the three zones of the CEMA classification is quantified in Fig. 7 (b). The histograms in the figure are obtained by the accumulation of reaction rate value of H_2 conditioned on α in the domain. The graph reveals that most of the fuel (approximately 80%) is consumed by auto-ignition in the bulk flow. To the authors' knowledge this is the first CEMA based quantification of the relative importance of auto-ignition versus flame propagation in the sequential combustor configuration.

4.2. Intermittent auto-ignition in mixing duct

Periodically, intermittent auto-ignition events that take place in the mixing duct immediately upstream of the area change are observed on a characteristic time scale $t_{AI} \sim 0.2ms$. An instantaneous description of such an event is reproduced qualitatively in Fig. 8 by the heat release rate, temperature and HO_2 mass fraction scalar fields. Quantities are normalized in the same manner as in Fig. 5. The spatially distributed, sudden ignition of a relatively vast fluid parcel, spanning the mixing duct from boundary layer to boundary layer, is clearly visible in the plots. The shape of the HO_2 iso-contours reveal that auto-ignition takes place in a pre-existing pool of HO_2 radicals convected from upstream. The observed auto-ignition behavior is in good accordance with experimental evidence of auto-ignition in the mixing duct

This is the accepted version of an article published in Proceedings of the Combustion Institute.
DOI: 10.1016/j.proci.2018.06.084

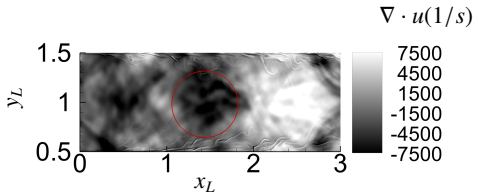

Figure 9: Contours of the instantaneous dilatation field ($\nabla \cdot u$) illustrating the wave pattern in a 2-D slice of the mixing duct (block 1 at the midplane in the spanwise direction). The red circle highlights a darker region of relatively high compression (negative dilatation).

at an equivalence ratio of 0.35 and for H_2 content above 76% in the fuel blends investigated in [4].

The nominal operating condition of the model sequential combustor simulated in the present study should not allow for auto-ignition to take place in the mixing duct due to its short characteristic residence time compared to the ignition delay time of the fuel mixture ($t_{mix} \sim 0.15ms < t_{ign} \sim 0.2ms$). Therefore, a tentative explanation of the observed behavior is provided. The presence of the flame at its design position effectively represents an active source of pressure fluctuations located downstream of the mixing duct and the area change: the flame induces local volumetric expansion of the auto-igniting fluid and this causes, in turn, compression waves traveling downstream towards the domain exit and, more importantly, upstream towards the domain inlet. The longitudinal component of these pressure fluctuations and their transverse components, reflected by the mixing duct walls, are able to intermittently converge forming a constructive interference pattern near the channel centerline. This is qualitatively illustrated in Fig. 9 by the instantaneous dilatation field. The transient pressure rise, in its upstream displacement, is coupled isentropically to a positive temperature fluctuation at the same location. Although relatively small, at approximately 20–30 K above the inlet conditions, this temperature fluctuation ultimately results in the appearance of early auto-ignition kernels in the mixing duct due to the strong temperature sensitivity of the hydrogen-air mixture's ignition delay time t_{ign} at elevated preheat temperatures.

Additional two-dimensional, geometrically simplified DNS of channel flow configurations covering a range of inlet temperatures and compositions were performed to support the explanation of the transient auto-ignition events described above. Results from these auxiliary studies (not shown here) have confirmed the key role of the isentropic pressure-temperature coupling in the transient upstream displacement of auto-ignition fronts.

5. Conclusions

A three-dimensional direct numerical simulation of a model sequential combustor at reheat conditions has been performed to understand the flame stabilization mechanism. Results from the simulation show the presence of two combustion states. In the primary design combustion state, where a triangular-shaped reaction zone is observed, the fuel is oxidized by auto-ignition along the centerline and flame propagation near the corners of the area change. The flame propagation mode is enabled by the recirculation created due to the sudden expansion of the cross-sectional geometry between the mixing duct and the combustion chamber. An indicator, based on a chemical explosive mode analysis (CEMA), has been used to distinguish these two modes of combustion and to quantify their contribution towards fuel consumption. It was found that the bulk of the fuel is consumed due to autoignition. A secondary combustion state in the sequential combustor is found to exist because of intermittent early auto-ignition events occurring in the mixing duct, which is caused by the extremely high temperature sensitivity of the ignition delay time for hydrogen-air mixtures. Several planned follow-up studies will investigate the model sequential combustor, first presented here, with the aim to: 1) understand the global flame response to variations in the reactants' reactivity; 2) quantify the effect of wall heat loss on the contribution of flame propagation to the stabilization of the combustion process; and 3) characterize the effect of pressure on the relative importance of auto-ignition versus flame propagation.

Acknowledgments

This publication has been produced with support from the NCCS Centre, performed under the Norwegian research program Centres for Environment-friendly Energy Research (FME). The authors acknowledge the following partners for their contributions: Aker Solutions, ANSALDO Energia, CoorsTek Membrane Sciences, Gassco, KROHNE, Larvik Shipping, Norcem, Norwegian Oil and Gas, Quad Geometrics, Shell, Statoil, TOTAL, and the Research Council of Norway (257579/E20). The computational allocation for the present study was provided by NERSC - the National Energy Research Scientific Computing Center in the United States - and by UNINETT Sigma2 - the National Infrastructure for High Performance Computing and Data Storage in Norway (project number nn9527k). The work at Sandia was supported by the US Department of Energy, Office of Basic Energy Sciences, Division

This is the accepted version of an article published in Proceedings of the Combustion Institute.
DOI: 10.1016/j.proci.2018.06.084

of Chemical Sciences, Geosciences, and Biosciences. Sandia National Laboratories is a multi-mission laboratory managed and operated by National Technology and Engineering Solutions of Sandia, LLC.,a wholly owned subsidiary of Honeywell International, Inc., for the U.S. Department of Energys National Nuclear Security Administration under contract DE-NA-0003525. The views expressed in the article do not necessarily represent the views of the U.S. Department of Energy or the United States Government.

References

[1] F. Güthe, J. Hellat, P. Flohr, Journal of Engineering for Gas Turbines and Power 131 (2009) 021503.

[2] D. A. Pennel, M. R. Bothien, A. Ciani, V. Granet, G. Singla, S. Thorpe, A. Wickstroem, K. Oumejjoud, M. Yaquinto, in: Proceedings of the ASME Turbo Expo 2017, June 26-30 2017, Charlotte (NC), USA, American Society of Mechanical Engineers, 2017, pp. GT2017–64790.

[3] T. Wind, F. Güthe, K. Syed, in: Proceedings of the ASME Turbo Expo 2014, June 16-20 2014, Düsseldorf, Germany, American Society of Mechanical Engineers, 2014, pp. GT2014–25813.

[4] J. Fleck, P. Griebel, A. M. Steinberg, M. Stöhr, M. Aigner, A. Ciani, in: Proceedings of the ASME Turbo Expo 2010, June 14-18 2010, Glasgow, Scotland, American Society of Mechanical Engineers, 2010, pp. GT2010–22722.

[5] J. Fleck, P. Griebel, A. M. Steinberg, M. Stöhr, M. Aigner, A. Ciani, Journal of Engineering for Gas Turbines and Power 134 (2012) 041502–1.

[6] J. M. Fleck, P. Griebel, A. M. Steinberg, C. M. Arndt, C. Naumann, M. Aigner, Proceedings of the Combustion Institute 34 (2013) 3185–3192.

[7] M. Poyyapakkam, J. Wood, S. Mayers, A. Ciani, F. Güthe, K. Syed, in: Proceedings of the ASME Turbo Expo 2012, June 11-15 2012, Copenhagen, Denmark, American Society of Mechanical Engineers, 2012, pp. GT2012–69165.

[8] M. Brower, E. L. Petersen, W. Metcalfe, H. J. Curran, M. Füri, G. Borque, N. Aluri, F. Güthe, Journal of Engineering for Gas Turbines and Power 135 (2013) 021504–1.

[9] O. Schulz, T. Jaravel, T. Poinsot, B. Cuenot, N. Noiray, Proceedings of the Combustion Institute 36 (2017) 1637–1644.

[10] R. Cabra, T. Myhrvold, J. Chen, R. Dibble, A. Karpetis, R. Barlow, Proceedings of the Combustion Institute 29 (2002) 1881–1888.

[11] C. S. Yoo, R. Sankaran, J. H. Chen, Journal of Fluid Mechanics 640 (2009) 453–481.

[12] Y. Yang, N. Noiray, A. Scarpato, O. Schulz, K. M. Düsing, M. R. Bothien, in: Proceedings of the ASME Turbo Expo 2015, June 15-19 2015, Montreal, Canada, American Society of Mechanical Engineers, 2015, pp. GT2015–42622.

[13] A. Scarpato, L. Zander, R. Kulkarni, B. Schuermans, in: Proceedings of the ASME Turbo Expo 2015, June 13-17 2016, Seoul, South Korea, American Society of Mechanical Engineers, 2016, pp. GT2016–.

[14] M. R. Bothien, D. Lauper, Y. Yang, A. Scarpato, in: Proceedings of the ASME Turbo Expo 2017, June 26-30 2017, Charlotte (NC), USA, American Society of Mechanical Engineers, 2017, pp. GT2017–64188.

[15] O. Schulz, N. Noiray, Combustion and Flame 192 (2018) 86 – 100.

[16] J. H. Chen, A. Choudhary, B. de Supinski, M. DeVries, E. R. Hawkes, S. Klasky, W. K. Liao, K. L. Ma, J. Mellor-Crummey, N. Podhorszki, R. Sankaran, S. Shende, C. S. Yoo, Computational Science & Discovery 2 (2009) 015001.

[17] C. A. Kennedy, M. H. Carpenter, Applied Numerical Mathematics 14 (1994) 397–433.

[18] C. A. Kennedy, M. H. Carpenter, R. M. Lewis, Applied Numerical Mathematics 35 (2000) 177–219.

[19] T. Poinsot, S. K. Lele, Journal of Computational Physics 101 (1992) 104–129.

[20] A. Gruber, P. S. Salimath, J. H. Chen, International Journal of Hydrogen Energy 39 (2014) 5906–5918.

[21] A. Gruber, R. Sankaran, E. R. Hawkes, J. H. Chen, Journal of Fluid Mechanics 658 (2010) 5–32.

[22] A. Gruber, J. H. Chen, D. Valiev, C. K. Law, Journal of Fluid Mechanics 709 (2012) 516–542.

[23] A. Gruber, A. R. Kerstein, D. Valiev, C. K. Law, H. Kolla, J. H. Chen, Proceedings of the Combustion Institute 35 (2015) 1485–1492.

[24] J. Li, Z. Zhao, A. Kazarov, F. L. Dryer, International Journal of Chemical Kinetics 36 (2004) 566–575.

[25] R. Gordon, A. Masri, S. Pope, G. Goldin, Combust. Flame 151 (2007) 495–511.

[26] T. F. Lu, C. S. Yoo, J. H. Chen, C. K. Law, Journal of Fluid Mechanics 652 (2010) 45–64.

[27] R. Shan, T. F. Lu, Combustion and Flame 159 (2012) 2069–2076.

[28] C. Xu, J.-w. Park, C. S. Yoo, J. H. Chen, T. Lu, Proceedings of the Combustion Institute (2018). In press.

This is the accepted version of an article published in Proceedings of the Combustion Institute.
DOI: 10.1016/j.proci.2018.06.084